Controlling association and separation of gold nanoparticles with computationally designed zinc-coordinating proteins

Matthew J. Eibling[‡,a], Christopher M. MacDermaid[‡,a,c], Zhaoxia Qian[a,d], Christopher J. Lanci[a,e], So-Jung Park*[,a,b], Jeffery G. Saven*[,a]

AUTHOR ADDRESS

a. Department of Chemistry, University of Pennsylvania, Philadelphia PA 19104

b. Department of Chemistry and Nanoscience, Ewha Womans University, Seoul, 03760, South Korea

ABSTRACT. Functionalization of nanoparticles with biopolymers has yielded a wide range of structured and responsive hybrid materials. DNA provides the ability to program length and recognition using complementary oligonucleotide sequences. Nature more often leverages the versatility of proteins, however, where structure, assembly, and recognition are more subtle to engineer. Herein, a protein was computationally designed to present multiple Zn^{2+} coordination sites and cooperatively self-associate to form an antiparallel helical homodimer. Each subunit was unstructured in the absence of Zn^{2+} or when the cation was sequestered with a chelating agent. When bound to the surface of gold nanoparticles via cysteine, the protein provided a reversible molecular linkage between particles. Nanoparticle association and changes in interparticle separation were monitored by redshifts in the surface plasmon resonance (SPR) band and by transmission electron microscopy (TEM). Titrations with Zn^{2+} revealed sigmoidal transitions at submicromolar concentrations. The metal-ion concentration required to trigger association varied with the loading of the proteins on the nanoparticles, the solution ionic strength, and the cation employed. Specifying the number of helical (heptad) repeat units conferred control over protein length and nanoparticle separation. Two different length proteins were designed via extension of the helical structure. TEM and extinction measurements revealed distributions of nanoparticle separations consistent with the expected protein structures. Nanoparticle association, interparticle separation, and SPR properties can be tuned using computationally designed proteins, where protein structure, folding, length, and response to molecular species such as Zn^{2+} can be engineered.

Introduction

Nano-scale hybrid materials combine "hard" nanomaterials such as inorganic nanoparticles (NPs) and "soft" materials such as polymers. Potential applications include sensing[1], imaging[2], catalysis[3], self-assembling materials[4], drug-delivery[5], and plasmonic devices[6]. These hybrid systems can incorporate polymers or biopolymers such as deoxyribonucleic acids (DNA) and proteins in combination with NPs. The key feature of the biological components of these systems is that they are programmable, where variation of the biopolymer subunits results in variation of structure and functionality. This functionality can be further tuned by choosing the size, shape, and composition of NPs to incorporate desirable optical, electronic, or magnetic properties.[7-12] Programmability of DNA-functionalized NPs is straightforward, where base-pair complementarity allows hybridization of complementary DNA strands. It is also of interest to consider other biopolymers, particularly those having greater structural and functional diversity such as proteins. However, the interactions of proteins are more subtle and challenging to design. Herein we discuss the tailoring of a protein biopolymer to achieve a hybrid-NP material whose assembly is triggered by the presence of Zn^{2+} ions.

In the past, gold nanoparticles (AuNPs) have been functionalized with small molecules, polymers, and biopolymers. Without proper surface passivation, [13-14] [15-18] NPs undergo irreversible aggregation under most biologically relevant solution conditions.[19] While small molecules confer such surface passivation, they typically offer limited control over the assembly structures of NPs.[20-22] Functionalizing NPs with biopolymers, particularly those having a degree of programmability, affords the capability to generate specific interactions. Complementary strands of DNA have been used to mediate assembly of metal NPs into well-defined small clusters[23], macroscopic aggregates[24], layered structures[25-27], three-dimensional superlattices[28-29], and complex nanostructures[30-32]. Of specific interest has been the control of NP spacing and reversible assembly.[24, 33-36] DNA linkers can yield a broad range of interparticle separation distances[24, 33, 36] with assembly triggered by changes in system conditions.[37-39] The control over separation provided by DNA has been used to study distance dependent phenomena such as energy transfer

between nanoparticles[40-41] and sensing DNA-binding proteins.[42-49]

Compared to DNA, proteins have a greater number of monomer types (amino acids) and are more versatile structurally and functionally. Moreover, proteins can be stable in a wide array of solvent conditions and can be tuned for stability in a chosen salt and pH environment. Work has proceeded in this area by combining NPs with well-structured natural proteins to control the assembly of NPs[50-56], develop sensors of metal ions[57] and biological molecules[58-59], and modulate enzymatic and biological activity[60-61]. Protein-NP systems can leverage the structures and functions of proteins to realize association of nanoparticles in one, two, and three dimensions.[62-67] Proteins adhered to nanoparticles have been used to control NP assembly via association of their unfolded states.[68-69] Electrostatic interactions involving proteins and nanoparticles have also been used to control NP association.[70-71] Specific, selective interactions involving proteins attached to nanoparticles can confer nanoparticle association, e.g., using antigen-antibody pairs[72-73] and biotin-streptavidin systems.[74] With protein functionalized nanoparticles, association can be controlled via variation of pH[70, 75-76], electrostatic interactions [71], and relative concentrations of peptides and nanoparticles.[77] Protein-protein interactions offer great promise for tunable association of protein-NP systems. Dimeric coiled-coil proteins have been used to mediate association of nanoparticles, and the dimerization can be reversed with variation of pH.[78] Triggering association under conditions which do not involve variation of pH or temperature is relevant for a wide variety of applications, including biomolecular sensing. Use of a mediator that triggers protein association is one such approach. A ternary helical coiled-coil system has been developed, where particles are functionalized with two distinct peptides, and the addition of a third yields association which can be reversed via the use of denaturant.[79] With a designed protein that forms a dimer in the presence of metal ions, nanoparticle association can be reversibly controlled via addition and sequestration of these metal ions.[80-82] These previous efforts highlight the capabilities of proteins and peptides to mediate and control nanoparticle association.

Generalizing this protein-NP approach, however, presents substantial challenges associated with designing proteins given their size, large number of possible sequences, and the subtle intermolecular interactions that confer folding and assembly.[83-87] Consequently, current protein-NP hybrid systems commonly use structures and structural motifs found in natural proteins. When more precise control of structure and function is desired, such as tunability of length and association conditions, it is advantageous to design a protein system from scratch. In such cases, computational design affords the ability to go beyond natural systems and instead build, from the ground up, a unique protein programmed with the desired functionality.[88-92] The effort herein involves the metalloprotein design, which has received substantial attention.[83-87, 93-97]

An important next step is to develop NP-protein systems that integrate and extend current capabilities to allow (a) reversible control of the association of protein-functionalized particles, (b) nanoparticle dispersion over a range of ionic strengths and buffer conditions, (c) programmable control of interparticle spacing, (d) assembly and disassembly at neutral pH and room temperature, and (e) use of metal ion mediators to elicit association at low (micromolar) concentrations. We present a protein-NP system that achieves these capabilities using a computationally designed helical dimer having multiple zinc-coordinating sites.

Experimental Methods

Protein Synthesis and Purification. Designed amino acid sequences were synthesized via solid phase synthesis, purified by reversed phase HPLC, and characterized by MALDI-MS. (For details see Supporting Information.)

Au Nanoparticle Preparation. Spherical AuNPs were synthesized by the Turkevich method.[98] (For details see Supporting Information.) The aggregation state of the particles is sensitive to solution ionic strength. Cations of different size and charge have different effectiveness at screening the negative charge of citrate resulting in irreversible aggregation of AuNPs.[99-101] For example, 3 nM citrate capped AuNPs in 10 mM 3-(N-morpholino)propanesulfonic acid (MOPS) pH 7 were found to irreversibly aggregate with the addition of 200 μM Zn^{2+} and Ca^{2+}. Citrate capped AuNPs are typically stable in 10 mM Na^{+}.[101] As such, care was taken to select a low ionic strength 10 mM MOPS pH 7 buffer (Sigma-Aldrich). Both the protein and AuNPs were found to remain dispersed in this buffer.

Citrate capped AuNPs in 10 mM MOPS pH 7 buffer were characterized with UV-Vis spectroscopy and small angle x-ray scattering (SAXS). SAXS measurements revealed an AuNP diameter of 13.5 ± 1.6 nm. (For details see Supporting Information.) UV-Vis measurements revealed the surface plasmon resonance (SPR) wavelength of maximum extinction (λ_{max}) to be 520 nm, which is consistent with 13 nm AuNP diameter.[102-104]

Protein/NP Complex Preparation. All ligand exchange reactions were performed in a 10 mM MOPS pH 7 buffer. Unless indicated otherwise, this buffer system was used for all solution-phase studies. Each mixing step was performed in a 1.5 mL centrifuge tube resting in a 50 mL conical vial, which was fixed to the tray of an incubator shaker rotating at 250 rpm and 25°C.

Ligand exchange reactions were performed in 1 mL volumes. In the first step, 3.98 μM of protein was treated with a stoichiometric amount of pH 7 tris(2-carboxyethyl)phosphine (TCEP) and mixed for 1 hour to ensure cysteine residues are present as the reduced (thiol) form. This was followed by addition of citrate capped NPs to achieve a 3 nM NP solution. The solution was then mixed for 16 hours. During this time, the thiol group of cysteine displaces the weakly associated citrate ions and coordinates to the AuNP surface.[105] The resultant protein ligated NPs were purified from the unbound protein in solution by three consecutive centrifugation steps consist-

ing of 40 minutes at 13,400 rcf. After each centrifugation step, 950 μL of supernatant was replaced with 10 mM MOPS pH 7 buffer, and the NPs were resuspended in buffer by vortexing. The UV-Vis spectrum of the supernatant from the final centrifugation step confirmed the absence of free protein.

Two protein loading variants were made. A higher loading variant prepared with a ligand exchange composition [Cysteine : NP : Protein] having the relative molar ratios [0 : 1 : 1325]; the concentration of each species was [0 : 3 nM : 3.98 μM], respectively. A lower loading variant was also created with ligand exchange composition of [2500 : 1 : 1325] using the following concentrations of each species [7.5 μM : 3 nM : 3.98 μM]. Cysteine was treated with TCEP in the same manner as the protein. To achieve a lower loading, the NPs were first combined with cysteine and mixed for 16 hours prior to the addition of proteins.

The amounts of proteins on nanoparticles (loadings) were determined by fluorescence measurements of protein (Supporting Information, Figure S1), which was cleaved from the surface of AuNPs by the addition of 10 mM dithiothreitol (DTT) and mixing overnight at room temperature. During this time, the mono-thiol protein is replaced by the more strongly binding di-thiol DTT.[106-108] The samples were then centrifuged at 12,000 rpm for 30 minutes thereby removing the DTT substituted AuNPs. The concentration of free protein in the supernatant was then determined by measuring tyrosine fluorescence. The protein contains a tyrosine residue that was excited at 275 nm. The collected emission spectra, with maxima at 305 nm, were compared against a calibration curve of known concentrations of the protein in the presence of 10 mM DTT. Over time, DTT is oxidized, and oxidized DTT acts as a static quencher of tyrosine.[109] To avoid error, all surface loading samples and calibration curve samples were prepared and analyzed at the same time. In addition, the concentration of DTT was more than 1000 times that of the AuNP, such that the effect of DTT binding to the AuNP surface would have negligible impact to the DTT concentration left in the supernatant.

Stock solutions of 250 μM Zn^{2+} and 25 μM Zn^{2+} were prepared from $ZnSO_4 \cdot 7H_2O$ (Acros Organics) in 18.2 MΩ·cm resistivity water. EDTA Stock solutions (250 μM and 25 μM) were prepared by dilutions of a neutral pH 0.5 M EDTA solution (Gibco).

Spectroscopy. Protein and AuNP concentrations were measured in 1 cm path length quartz cuvettes (Starna) using a Cary 100 Bio UV-visible spectrophotometer in double beam mode. Shifts in AuNP SPR bands were monitored at room temperature using a TECAN Infinite M1000 PRO Plate Reader UV-visible spectrophotometer and Greiner bio-one 384 well μClear non-binding microplates. Circular dichroism (CD) measurements were performed in Starna 0.1 cm path length quartz cuvettes using an AVIV Circular Dichroism Spectrometer Model 410. Isothermal wavelength scans were collected at 20°C. Unless indicated otherwise, error bars associated with λ_{max} in titrations are plus/minus one standard deviation, where the standard deviation is calculated using measurements from three independent preparations of protein functionalized AuNPs.

Analytical Ultracentrifugation (AUC). Sedimentation equilibrium AUC was performed using a Beckman Optima XL-I centrifuge, An-60 Ti rotor, and cells with a six-channel centerpiece and quartz windows. Absorbance data (280 nm) was collected at 4 °C and 18,000 26,000 and 34,000 rpm. A total equilibration time of 24 hours was used for each speed. Buffer for all samples consisted of 25 mM MOPS, 25 mM NaCl, pH 7.4. Holo samples of 40 μM, 60 μM, and 80 μM ZAD5-NoLinker protein each with 600 μM Zn^{2+} were analyzed. Partial specific volume of the protein (0.6951 cm^3/g) as well as the solvent density (1.0012 g/cm^3) were calculated from standard tables using the SEDNTERP program.[110] Data analysis was performed by global analysis of the nine data sets (three concentrations at three different speeds) using SEDPHAT (version 12.1b).[111] SEDPHAT's Species Analysis and Monomer-Dimer Self-Association models were used for global fits, and SEDPHAT's covariance matrix analysis was used to estimate error intervals.

Transmission Electron Microscopy (TEM). Samples to determine protein-mediated interparticle separations were prepared by adding 100 μM Zn^{2+} to 3 nM of protein-ligated AuNPs in a 500 μL centrifuge tube. The tube was flicked several times to mix and 10 μL of the solution was deposited on a TEM grid. The TEM grid was pre-positioned on an ozone cleaned piece of Si mounted to a spincoater. The sample was spun for 5 minutes at 2000 rpm. The sample preparation time between addition of Zn^{2+} and the start of the spincoater was approximately 25 seconds. The TEM grid was held in place on the Si plate by the surface tension of water. TEM characterization was done on a JEOL 2100 TEM.

Results and Discussion

Design of Protein Structure. Backbone structures were computationally designed to support a targeted Zn^{2+} binding motif. We leveraged previous work in parameterizing such "coiled-coil" structures, and each helix contained a seven-residue "heptad" repeat.[87, 112-113] Helical protein structures were created *de novo* subject to variation a small set of global geometric parameters.[88-89, 114-117] An ensemble of mathematically specified, dimeric D_2 symmetric coiled-coil structures was generated, where each structure comprised two antiparallel 35-residue alpha helices. From this ensemble, structures were selected that support inter-helical, bis-histidine zinc-coordinating sites.[118-119] Each coordinating site was solvent exposed, allowing for two solvent water molecules (not considered explicitly in the calculations) to complete the tetrahedral coordination of each zinc ion. The periodicity of the heptad repeat allows for the creation of dimeric structures having a specified number of putative zinc-coordinating sites (Figure 1b). Initially, structures having five coordination sites were considered. Structures so generated were energy minimized before performing subsequent sequence design. (A detailed description appears in the Supporting Information.)

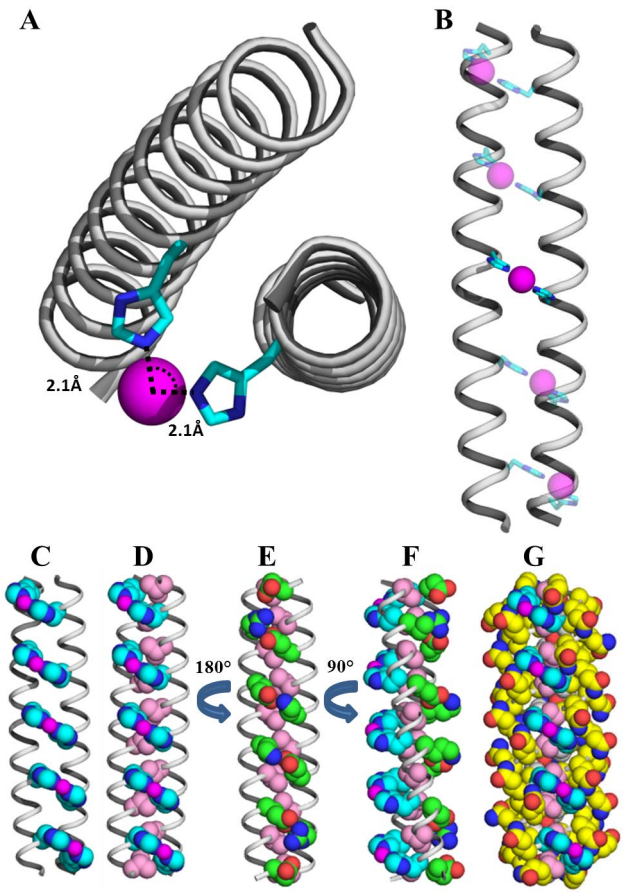

Figure 1. Designing ZAD5. (A) Computationally identified Zn^{2+} coordination site for ZAD5 with Zn^{2+} cation (magenta) and histidines (cyan, blue). The targeted Zn^{2+}- Nε2 bond length was 2.1 Å, and the targeted $N\varepsilon_{2a}$-Zn^{2+}-$N\varepsilon_{2a'}$ bond angle was 109.5°. (B) To create the 5-site model, the identified configuration in (A) was positioned at four *a-a'* heptad positions in the computationally generated coiled coil. (C) Five bis-histidine coordination sites of ZAD5 are rendered as space filling (cyan). (D) As in (C) with interior hydrophobic core residues, valines, rendered (pink). (E) Salt bridging side chains (green). (F) Histidine coordination sites (cyan, magenta) and salt bridges (green) appear opposite one another. (G) Remaining residues (yellow).

Sequence Design. To determine sequences, the probabilities of the amino acids were estimated computationally using a probabilistic approach.[86, 120-123] An atomistic potential energy function and discrete side chain conformations were employed using a rotameric state approximation.[124] The approach provides an average total internal energy over sequences consistent with a given structure and set of constraints. Separate sequence calculations were performed for each dimeric structure. The identified positions and conformations of the histidine residues were not allowed to vary. The sets of amino acids considered at the remaining positions were selected based upon the locations of the residues within the dimeric structure. The site-specific amino acid probabilities were determined through multiple iterations of probabilistic design, as described previously. [121-122, 125-126] A final calculation was used to calculate the average internal energy over the rotameric states of each final sequence. Multiple low internal energy sequence-structure combinations were identified. The lowest energy combination possessed a superhelical radius larger than observed in most natural dimeric coiled-coils, r = 5.2 *Å*: NQHYQ FQQEH QQVQQ EHQQV QQKHQ QLQQK HQQWQ. This sequence was synthesized and observed to dimerize in the presence of Zn^{2+} (Supporting Information, Figure S4). A separate low internal energy sequence-structure combination was observed for a structure having a smaller superhelical radius r = 4.6 Å, and a sequence was computationally identified and labeled ZAD5-NoLinker: NEHYQ VQQEH QQVQQ KHQQV QQEHQ YVQQR HQQVQ. In addition to the designed bis-His Zn^{2+} coordination sites, the model structure for this dimer possessed complementary hydrophobic interactions among interior valine residues and salt-bridge interactions across the helix-helix interface (Figure 1c, 1d, 1e, 1f). To create a construct suitable for attachment to AuNPs, a tri-glycine linker and cysteine residue were added to the C-terminus, resulting in the following sequence: NEHYQVQ QEHQQVQ QKHQQVQ QEHQYVQ QRHQQVQ GGGC. This sequence, a putative zinc-activated dimer containing five zinc-coordinating sites, was labeled ZAD5. (A more detailed description appears in the Supporting Information.)

Characterization of the Protein. ZAD5-NoLinker was characterized in 20 mM MOPS 50 mM NaCl pH 7.8 buffer by circular dichroism (CD) (Figure 2a). In the absence of Zn^{2+}, the mean residue ellipticity was consistent with that of a protein with little or no persistent secondary structure (random coil). In the presence of four equivalents of Zn^{2+}, minima in the mean residue ellipticity were observed at 208 and 222 nm, consistent with the formation of helical secondary structure.

CD spectroscopy was also used to monitor helical structure upon the addition of a zinc-chelating agent. The titrations in Figure 2b are for sequential additions of Zn^{2+} up to four equivalents, followed by sequential additions of ethylenediaminetetraaceticacid (EDTA). Subsequent addition of EDTA decreases the magnitude of the mean residue ellipticity at 222 nm. The sequestration of Zn^{2+} coincides with the loss of alpha helical structure. These observations are consistent with the reversible formation/loss of helical structure upon the addition/removal of Zn^{2+}.

Sedimentation equilibrium AUC was performed on holo ZAD5-NoLinker samples consisting of 40 μM, 60 μM, and 80 μM protein with 600 μM Zn^{2+} to determine the molecular weight and thereby oligomerization state of the Zn^{2+} associated species. Buffer conditions were 25 mM MOPS, 25 mM NaCl, pH 7.4 and chosen to be similar to those used for CD measurements with slightly lower pH to allow greater Zn^{2+} solubility. Global fits using SEDPHAT's single Species Analysis model revealed a molecular weight of 9378 ± 134 g/mol consistent with the calculated mass of 9,390 g/mol for the ZAD5-NoLinker dimer bound with 5 copies of Zn^{2+}. Additionally, SEDPHAT's Monomer-Dimer Self-Association model was applied to the holo samples, which revealed a monomer-dimer equilibrium with an apparent association constant

$\log_{10}(K_a/M)$ = 6.07 ± 1.83 and a fitted monomer mass of 4701 ± 315 g/mol. Given protein concentrations ranging from 40 µM to 60 µM, this association constant is consistent with the dimeric oligomerization state observed in the single Species Analysis fit. Furthermore, the fitted mass of the monomer (4701 ± 315 g/mol) is in agreement with half the mass of the calculated holo dimer (4695 g/mol). The data strongly support a Zn^{2+} activated equilibrium comprising only monomer and dimer (no appreciable populations of higher molecular weight species). The AUC data for the samples fitted with SEDPHAT's Monomer-Dimer Self-Association model are shown in the Supporting Information, Figure S2.

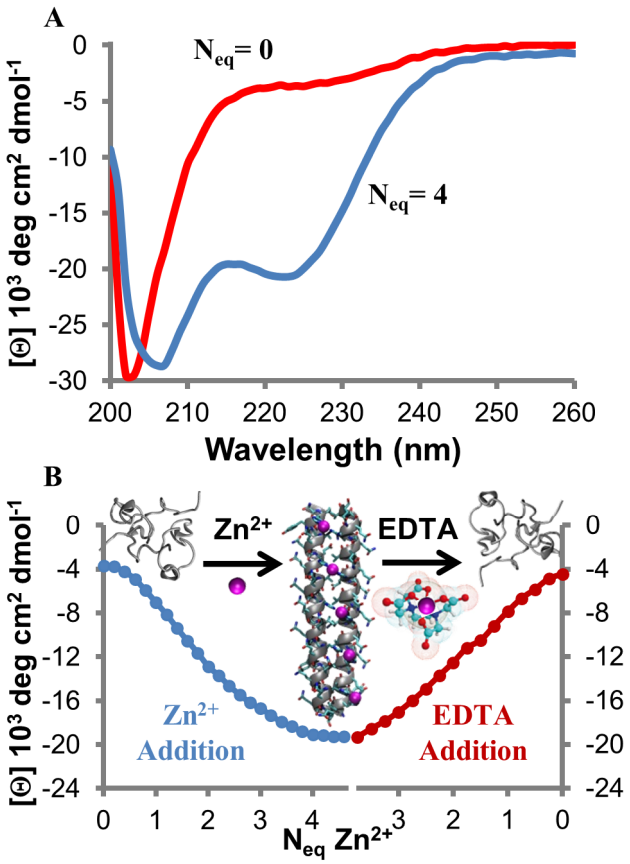

Figure 2. CD Spectroscopy of ZAD5-NoLinker. (A) Circular dichroism spectra with mean residue ellipticity of 40 µM Apo ZAD5-NoLinker (red) and 40 µM protein with 400 µM Zn^{2+} (blue). (B) Mean residue ellipticity of 40µM protein at 222 nm with increasing concentrations of Zn^{2+} (blue) and sequential additions EDTA (red). The number of equivalents Zn^{2+} is $N_{eq} = (2/5)([Zn]_{available}/[Protein])$, where $[Zn]_{available} = ([Zn]_{Total} - [EDTA])$. All measurements were performed at 20˚C.

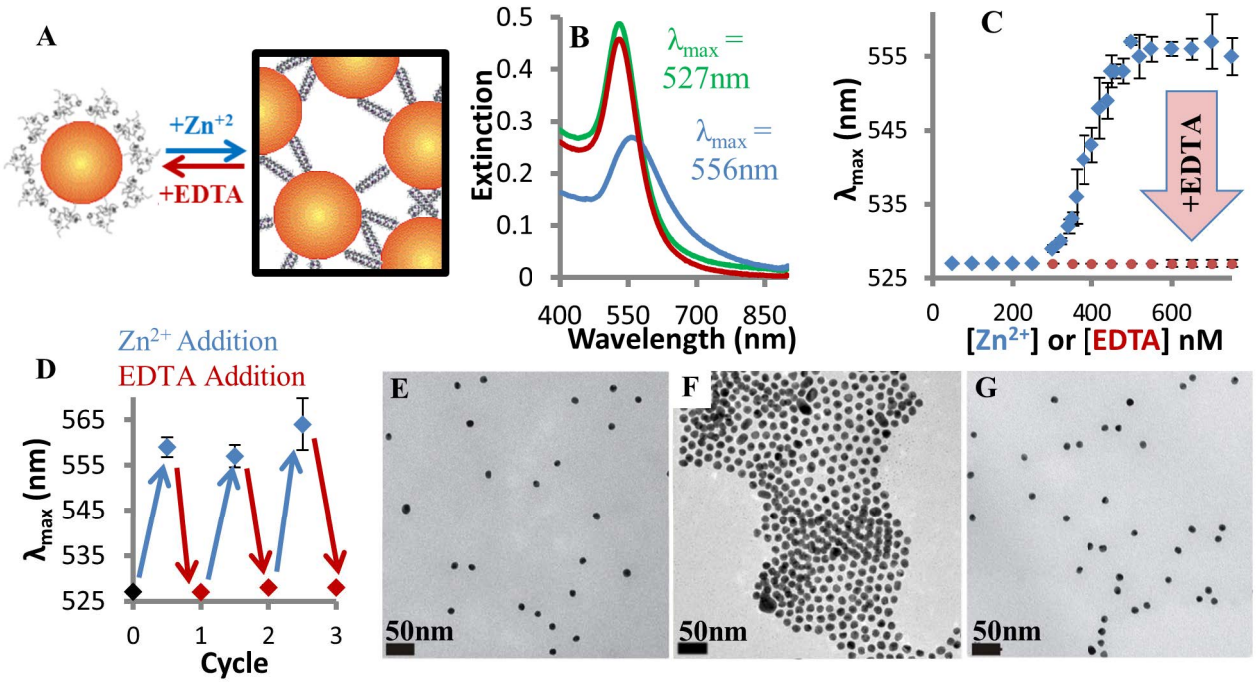

Figure 3. ZAD5-AuNPs in Free and Aggregated states. (A) Descriptive scheme showing the reversible assembly of protein coated AuNPs induced by zinc ion and EDTA. (B) UV-Vis spectra: 3 nM Apo ZAD5-AuNP (green curve); assembled with addition of Zn^{2+} ($ZnSO_4$), 3 nM ZAD5-AuNP and 400 μM Zn^{2+} (blue curve); and disassembled by stoichiometric addition of EDTA, 3 nM ZAD5-AuNP, 400 μM Zn^{2+} and 400 μM EDTA (red curve). Wavelengths of maximum extinction λ_{max} are indicated. (C) λ_{max} of a 3 nM ZAD5-AuNP solution at different Zn^{2+} concentrations (blue) and after subsequent addition of a stoichiometric amounts of EDTA, [EDTA] = [Zn^{2+}] (red). D) λ_{max} of a 3nM ZAD5-AuNP solution upon multiple cycles of increasing "available" zinc concentration, [Zn^{2+}]-[EDTA] = 2 μM (blue), followed by a stoichiometric addition of EDTA (red); at cycle 0, [EDTA] = 0. TEM of (E) Apo ZAD5-AuNP; (F) ZAD5-AuNP aggregates induced by addition of 100 μM Zn^{2+}, and (G) ZAD5-AuNP disassembled by addition of a stoichiometric quantity (100 μM) of EDTA. Error bars in (C) and (D) indicate plus/minus one standard deviation.

Characterization of protein functionalized AuNP. ZAD5 ligated AuNPs were prepared with two different surface loadings as described in the Methods section. The loading of the protein on NPs was determined by dissociating the protein from the NP using dithiothreitol (DTT) and measuring the protein concentration using fluorescence spectroscopy. The samples where ZAD5 was allowed to replace citrate directly, "ZAD5-AuNP", were found to have a loading of approximately 100 protein/AuNP or 0.18 protein/nm². The samples where the AuNPs were first subjected to cysteine to partially block the surface, "ZAD5-AuNP-50", were found to have a reduced loading of approximately 50 protein/AuNP or 0.09 protein/nm². These AuNP surface loadings are similar to the 0.14 protein/nm² at pH 7 reported for a disordered modified GCN4 construct having the same GGGC linker and 39-residue length as the ZAD5 construct.[127] A trend of increasing redshift in the surface plasmon resonance (SPR) wavelength of maximum extinction λ_{max} with increasing amount of protein on AuNP surface was observed: λ_{max}(Citrate-AuNP) = 520 nm; λ_{max}(ZAD5-AuNP-50) = 525 nm; and λ_{max}(ZAD5-AuNP) = 527 nm. These differences in SPR redshift are consistent with variation in refractive index at the AuNP surface due to the presence of bound protein.[128-130]

The aggregation and precipitation of citrate-ligated AuNPs are known to be sensitive to ionic strength.[131] The ZAD5-AuNP solutions, however, were robust with respect to changes in salt concentration. Solutions containing 3 nM ZAD5-AuNP in 10 mM MOPS at pH7 were exposed overnight to 500 mM NaCl, 50 mM $CaCl_2$, and 50 mM $MgCl_2$. For each of these three solutions, no change was observed in the SPR extinction for the ZAD5 functionalized particles. Under each of these same conditions, a 3 nM Citrate-AuNP solution showed complete loss of extinction due to NP aggregation and precipitation. These observations also reveal that Ca^{2+} and Mg^{2+} cations do not trigger folding, association, and AuNP aggregation at 50 mM concentrations.

Characterization of ZAD5-AuNP response to Zn^{2+}. The protein is hypothesized to undergo a similar change in structure and dimerization state when in solution and when bound to the surface of an AuNP via a flexible GGGC linker. CD data for ZAD5-NoLinker in solution exhibits a structural transition from random-coil to alpha-helical conformation upon the addition of Zn^{2+}. AUC data for ZAD5-NoLinker in solution are consistent with the formation of a dimeric species upon the addition of Zn^{2+}. (See "Characterization of the Protein." section.) ZAD5-AuNP would then be expected to associate upon addition of Zn^{2+} to activate the dimerization, which could be reversed upon sequestration of the metal ion with the addition of EDTA (Figure 3a).

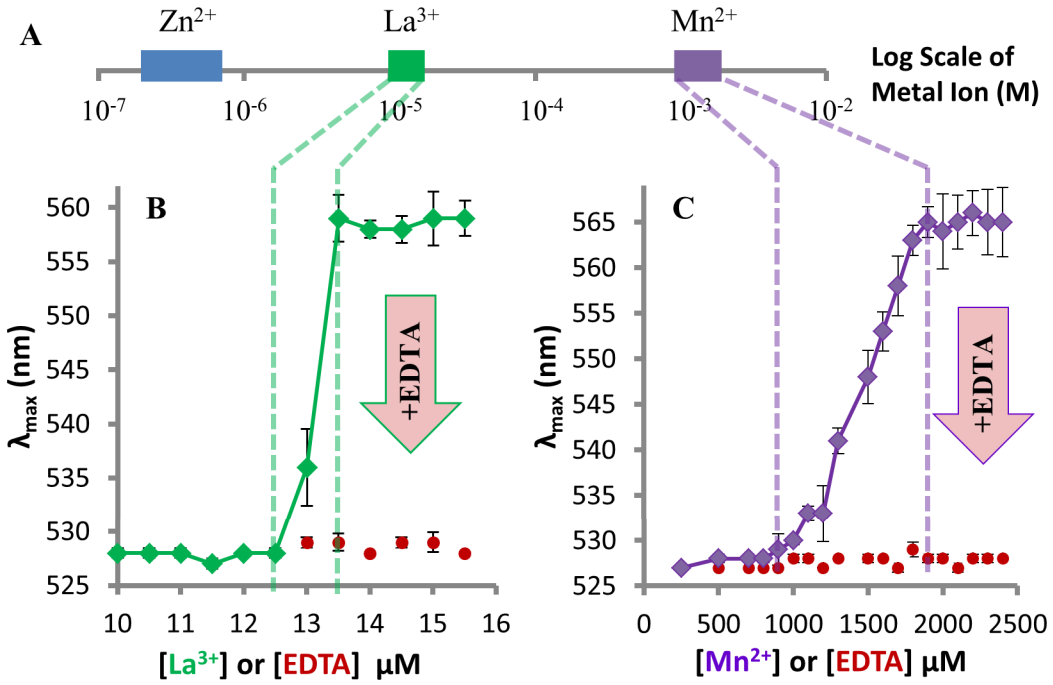

Figure 4. Association sensitivity to Zn^{2+}, La^{2+}, and Mn^{2+}. (A) Concentration ranges (transition windows) of different metal ions which induce assembly of 3 nM ZAD5-AuNPs. (B-C) λ_{max} of a 3 nM ZAD5-AuNP solution as a function of the concentration of La^{3+} (B) and Mn^{2+} (C). λ_{max} after addition of EDTA to achieve [La^{3+}] = [EDTA] (B) and [Mn^{2+}] = [EDTA] (C) are indicated in red. Dashed lines denote transition window associated with each metal ion in scheme (A) with the concentration ranges of assembly shown in (B-C). Data for Zn^{2+} appears in Fig. 3c. Error bars indicate plus/minus one standard deviation.

UV-Vis spectra may be used to monitor shifts in λ_{max} (Figure 3b, 3c, 3d). These SPR redshifts are indicative of changes in the NP separation distance.[79, 132-133] Dispersed ZAD5-AuNPs have a maximum SPR extinction wavelength at λ_{max} = 527 nm (Figure 3b green curve). Addition of Zn^{2+} causes a redshift to λ_{max} = 556 nm (Figure 3b, blue curve). The redshift is indicative of a decrease in the separation between the NPs in solution. The broadening of the SPR extinction band is also observed, which is consistent with increased scattering of the incident light by large aggregates of nanoparticles. The trends in extinction shift and broadening are well known in aggregated AuNP systems.[133-134]

The shift in λ_{max} was resolved as a function of Zn^{2+} concentration for 3 nM ZAD5-AuNP (Figure 3C). The λ_{max} exhibits a sharp sigmoidal transition with increasing metal-ion concentration, having a transition window midpoint near 400 nM Zn^{2+}. The width of the transition window spans approximately 300 nM (250 nM – 550 nM). This switch-like behavior is attributed to the cooperativity between the multiple metal binding sites of the homodimer as well as cooperativity involving the formation of multiple homodimers across one or more adjacent NP interfaces. As a control, comparable Zn^{2+} titrations were performed using ZAD5-NoLinker and citrate capped AuNP solutions, and no shifts in λ_{max} were observed (Figure S5).

Zinc-aggregated samples of ZAD5-AuNP could be reversibly dispersed with stoichiometric additions of EDTA. This is evidenced in the UV/Vis extinction by a return of λ_{max} and the peak width to values observed prior to Zn^{2+} addition. (Figure 3B red curve, and Figure 3C red points). The reversibility was tested over several cycles and monitored spectroscopically. The results shown in Figure 3D indicate that the system is capable of multiple cycles of association and dispersion, with little variation in the λ_{max} of the aggregated state and the EDTA released state for each cycle. The reversibility was also shown directly by transmission electron microscopy (TEM). Figure 3E presents a TEM sample with ZAD5-AuNPs in the absence of Zn^{2+} where the particles are freely dispersed. Figure 3F shows the aggregates observed after Zn^{2+} addition, and Figure 3G shows particles from a solution after a stoichiometric addition of EDTA to return the ZAD5-AuNPs to their dispersed state. The reversible nature of the system confirms the AuNP aggregation is protein and metal-ion mediated.

Characterization of ZAD5-AuNPs response to La^{3+} and Mn^{2+}. While ZAD5 was designed to coordinate Zn^{2+}, it is of interest to consider the selectivity of the metal-mediated association of ZAD5-AuNP. As mentioned previously, for 3 nM ZAD5-AuNPs, association was not observed in the presence of 50 mM Ca^{2+} and Mg^{2+}. La^{3+} and Mn^{2+} were also considered. La^{3+} was chosen because a previous study of a designed protein (also used to functionalize AuNPs) found that exposure to either Zn^{2+} or La^{3+} led to the formation of similar secondary structure content.[82] Mn^{2+} was chosen because a review of metalloproteins revealed that Zn^{2+} and Mn^{2+} binding sites often contain histidine residues.[135]

Titrations of La^{3+} and Mn^{2+} into 3 nM ZAD5-AuNPs revealed trends similar to those observed upon exposure to Zn^{2+}. (1) The SPR λ_{max} as functions of metal ion concentration were sigmoidal, exhibiting switch-like behavior. (2) The transitions were reversible by stoichiometric addition of EDTA. Notably different, however, were the larger metal ion concentrations required for ZAD5-AuNP association. Both metal ion concentration shifts were accompanied by decreasing sharpness of the sigmoidal transition and increases in the width of the transition windows. For 3 nM ZAD5-AuNP in 10 mM MOPS pH 7 buffer, Zn^{2+} activation occurred at 0.5 μM Zn^{2+} and had a transition window of 0.3 μM (0.250 μM – 0.550 μM) (Figure 3c). La^{3+} activation was centered at 13.5 μM La^{3+} and had a transition window of 1 μM (12.5 μM – 13.5 μM) (Figure 4b). Mn^{2+} activation occurred at 2000 μM Mn^{2+} and had a transition window of 1000 μM (900 μM – 1900 μM) (Figure 4c). The concentration ranges of these metal activated transition windows are depicted on a logarithmic scale in Figure 4a, revealing order of magnitude separations in the concentrations sufficient for nanoparticle association as well as pronounced selectivity for Zn^{2+} over La^{3+} and Mn^{2+}. When considering Zn^{2+} compared to Mn^{2+}, the observed binding trend agrees with the well-known Irving-Williams Series of relative stabilities of M^{2+} first-row transition metal ion complexes involving nitrogen-coordinating ligands.[136] [137] The ZAD5 metal binding site consists of inter-helical, bis-histidine residues positioned in a tetrahedral binding geometry. This is ideal for binding Zn^{2+}, which readily accommodates tetrahedral coordination environments. Conversely, in proteins, Mn^{2+} is primarily in octahedral geometries and only prefers tetrahedral coordination when fully saturated with negatively charged ligands.[138] The designed ZAD5 binding site does not present the preferred Mn^{2+} ligand geometry,[139] which is consistent with the observed selectivity for Zn^{2+} over Mn^{2+}. La^{3+} is relatively insensitive to ligand geometry.[140] This geometric consideration as well as the high oxidation state of La^{3+} may be responsible for the observed trend for the three metal ions. Further investigation is needed to understand the binding of Mn^{2+} and La^{3+}. These observations reveal that these metal ions expected to have little or no affinity for the putative bis-his coordination sites can elicit ZAD5-AuNP association at sufficiently high concentrations.

ZAD5-AuNP Zn^{2+} response in the presence of solution additives. As previously discussed, the designed protein includes three main sets of complementary interactions at the interhelical regions of the dimer: a hydrophobic valine zipper, salt-bridging interactions, and histidine-metal ion interactions. While the dimerization is metal-ion activated, the hydrophobic valine core and salt-bridging interactions also stabilize the alpha-helical dimer formation. As such, solution conditions which alter the strengths of these interactions should have an impact on the metal-ion concentration required to activate association of functionalized particles. Toward this end, we considered the Zn^{2+} response of ZAD5-AuNPs in the presence of solution additives.

The strength of salt-bridge interactions and the importance of their role in conferring structure within a protein are expected to decrease with increasing ionic strength. Particle association was monitored at two different salt concentrations: (a) 10 mM MOPS, pH 7 and (b) 10 mM MOPS, pH 7, and 153 mM NaCl. Condition (b) creates a saline pH 7 buffered environment often used with biological systems. The additional 153 mM NaCl is expected to partially shield the positive and negative charges of the Arg, Lys, and Glu residues. In Figure 5, the blue trace reveals the association of ZAD5-AuNPs in the higher ionic strength environment required more than 1 μM Zn^{2+}, which contrasts with only 0.5 μM Zn^{2+} when no NaCl is present. These observations are consistent with the destabilization of salt-bridging interactions at higher ionic strength conditions. The increase in solution ionic strength did not affect the reversibility of the system. As shown in the red trace of Figure 5, the association is still fully reversible with stoichiometric additions of EDTA. UV-Vis control experiments of 3 nM citrate capped AuNPs with 300 nM ZAD5-NoLinker in the presence of 153 mM NaCl resulted in irreversible AuNP aggregation. The ZAD5-NoLinker concentration corresponded to that of ZAD5 for 3nM ZAD5-AuNPs having a surface loading of approximately 100 protein/AuNP. This confirms ZAD5 only stabilizes the AuNPs in 153 mM NaCl when attached to the AuNP surface.

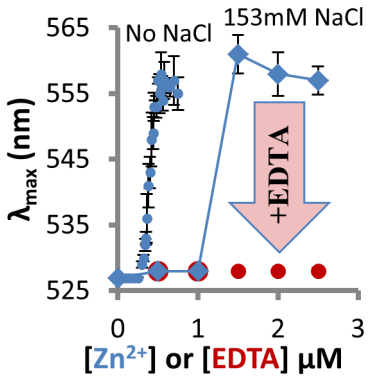

Figure 5. Zn^{2+} Titration of ZAD5–AuNPs in 153 mM NaCl. Wavelength of maximum extinction of a ZAD5-AuNP solution at increasing Zn^{2+} concentration. [NaCl] = 0 M (blue circle; see also Figure 3C). [NaCl] = 153 mM (blue diamond); after addition of EDTA (red), [EDTA] = [Zn^{2+}]. Error bars indicate plus/minus one standard deviation.

A decrease in the strength of the hydrophobic (valine zipper) interaction between the helices was achieved with increasing percent volume (v%) of trifluoroethanol (TFE). TFE was chosen because it is well-tolerated by proteins in solution and does not adversely affect helix formation when up to 80 v% TFE is present in solution.[141-143] In fact, TFE is well-known to enhance alpha helix formation of isolated non-associating single alpha-helices.[143] Thus, this cosolvent increases the hydrophobic character of the buffer system without the added complication of destabilizing helices. The Zn^{2+} dependent response of ZAD5-AuNP in 10 mM MOPS pH7 was examined at four different fractions of TFE: 0%, 20%, 40%, and 60% by volume. Increasing TFE content is expected to decrease the strength of the hydrophobic (valine) interaction within the interior of the dimer. Figure 6 shows an increase in the Zn^{2+} concentration required for dimerization as the v% of TFE in solution increases. This observation is consistent with ZAD5-AuNP association requiring a greater concentration of Zn^{2+} to compensate for destabilization of designed, complementary hydrophobic interactions within the helix dimer. The increase in v% TFE did not affect the reversibility of the system with respect to addition and sequestration of Zn^{2+}.

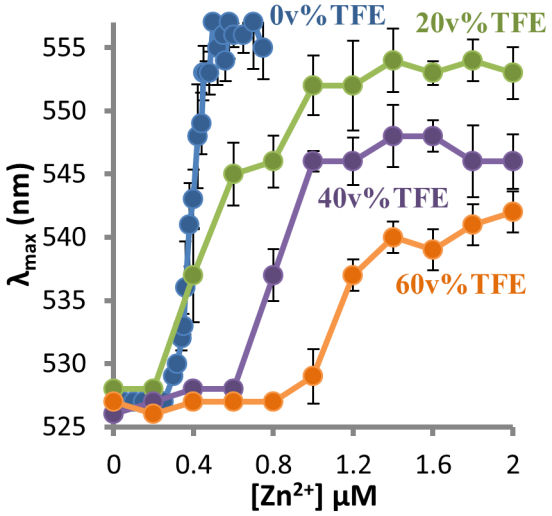

Figure 6. Zn^{2+} Titrations in presence of TFE. Wavelength at maximum extinction of ZAD5-AuNPs in solvent with different volume ratios of TFE upon addition of different concentrations of Zn^{2+}. Error bars indicate plus/minus one standard deviation.

Characterization of ZAD5-AuNP-50 response to Zn^{2+}. The lower protein loading ZAD5-AuNP-50 sample with approximately 50 protein/AuNP was also found to exhibit a reversible aggregation response in the presence of Zn^{2+}. Figure 7 shows a comparison of the Zn^{2+} response of the ZAD5-AuNP (~100 protein/AuNP) and ZAD5-AuNP-50 systems. For the same concentration of functionalized NPs (3 nM), the ZAD5-AuNP-50 system with lower loading requires a greater Zn^{2+} concentration to activate association. In addition, the concentration range (width) of the transition window is increased for the lower loading sample. These changes are potentially due to a reduced local protein concentration at the ZAD5-AuNP-50 surface resulting in fewer protein-mediated connections between the AuNPs. Nonetheless, both loadings still exhibit sigmoidal transitions indicative of cooperative binding interactions, similar redshifts in λ_{max}, and complete reversal to their zinc-free states by adding stoichiometric amounts of EDTA.

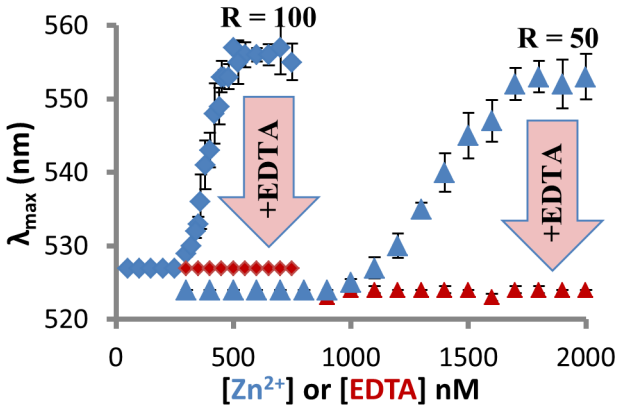

Figure 7. Protein loading dependent Zn^{2+} sensitivity. Wavelength at maximum extinction of ZAD5-AuNP (diamonds) and ZAD5-AuNP-50 (triangles) solutions at different Zn^{2+} concentrations (blue). After addition of EDTA (red); [EDTA] = [Zn^{2+}]. R is the estimated number of proteins per AuNP. R = 100 protein/NP (diamonds). R = 50 protein/NP (triangles). Error bars indicate plus/minus one standard deviation.

Characterization of ZAD7-AuNP response to Zn^{2+}. The folded ZAD5 protein design model is an anti-parallel homodimer, wherein each helix is built using a repeating heptad unit. The length of the dimer structure may be controlled via variation of the number of repeating heptad subsequences, each of which includes the histidine of the Zn^{2+} coordination site. In principle then, the separation between AuNPs can potentially be controlled by varying the length of the protein. In an effort to explore this potential, a seven-heptad sequence (ZAD7) was synthesized: NEHYQVQ QEHQQVQ QKHQQVQ QEHQQVQ QKHQQVQ QEHQYVQ QRHQQVQ GGGC. An additional two-heptad repeat unit (underlined) was inserted interior to the sequence in a manner that extended the pattern of bis-His coordination of Zn^{2+}, valine zipper packing, and complementary salt bridge pairing. (Figure 8)

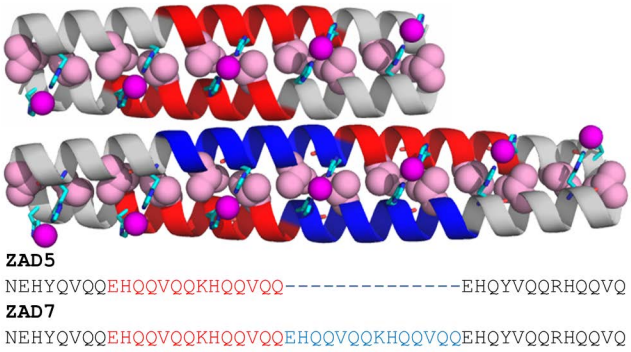

Figure 8. ZAD7 Protein. ZAD5 (Top) and ZAD7 (Bottom) proteins with heptad repeat units highlighted in red and blue. A 14-residue heptad subsequence (red) from ZAD5 is repeated and inserted (blue) to achieve ZAD7. ZAD7 contains two additional Zn^{2+} coordination sites while retaining valine core (pink) and salt-bridging interactions.

Using the same protocols to create ZAD5-AuNP, ZAD7 was introduced onto AuNPs yielding protein functionalized particles, ZAD7-AuNP. Titrations ranging from 0 nM to 750 nM Zn^{2+} in 50 nM increments were performed on solutions of 3 nM ZAD7-AuNP in 10 mM MOPS pH7 buffer. This data is shown overlaid with Zn^{2+} titrations of ZAD5 in Supporting Information (Figure S6). These titrations confirmed that 600 nM Zn^{2+} saturated both the ZAD5-AuNP and ZAD7-AuNP systems. In addition, the titration curves (Figure S6) show that the transition midpoints are similar for two systems, likely indicating similar affinity for Zn^{2+} consistent with a similar surface loading. In the absence of Zn^{2+}, the ZAD7-AuNP exhibits λ_{max} = 527 nm, which is identical to that of ZAD5-AuNP. This congruence is consistent with similar protein loadings for both the ZAD5-AuNP and ZAD7-AuNP systems on their NP surfaces. Upon exposure to 600 nM Zn^{2+}, the ZAD7-AuNP SPR band exhibited a redshift to λ_{max}(ZAD7-AuNP) = 544 nm; under similar conditions λ_{max}(ZAD5-AuNP) = 556 nm (Figure 3C). This 12 nm decrease in λ_{max} of the Zn^{2+} activated state is consistent with increased NP separation in the ZAD7-AuNP system.[79, 132-133] As with ZAD5-AuNP, the zinc-associated ZAD7-AuNP system was found to reversibly dissociate with the addition of stoichiometric amounts of EDTA, returning to λ_{max}(ZAD7-AuNP) = 527 nm. UV-Vis spectra of the apo and 600 nM Zn^{2+} ZAD5-AuNP and ZAD7-AuNP systems are shown in Supporting Information (Figure S7).

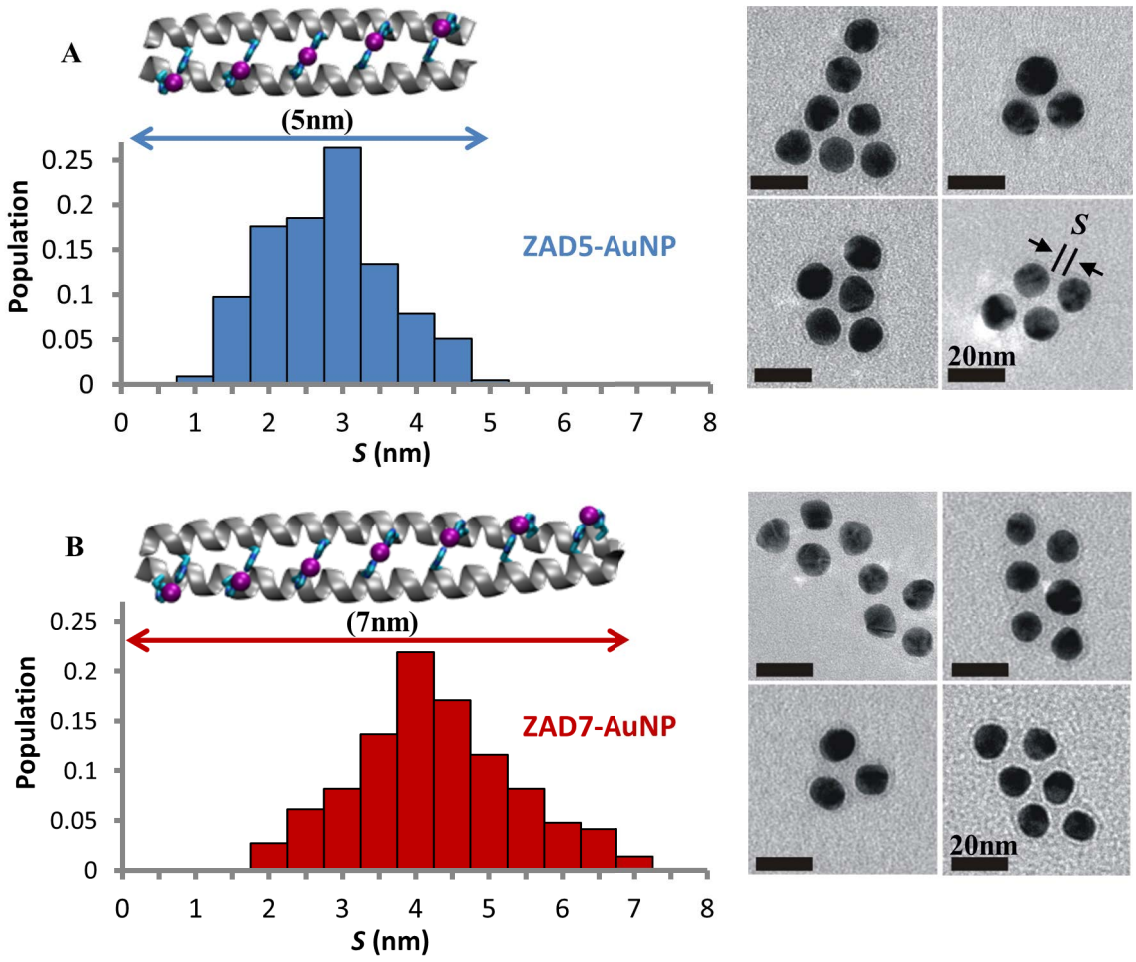

Figure 9. TEM studies of ZAD5-AuNP and ZAD7-AuNP. Histogram for interparticle separation *S* of (A) 216 (ZAD5-AuNP) and (B) 143 (ZAD7-AuNP) measurements obtained from TEM images of NP aggregates. Each centered bin of the histogram is 0.5 nm wide. Renderings of ZAD5 and ZAD7 are on the same length scale as the histogram abscissa. To the right of each histogram are representative TEM images used for the interparticle separation (*S*) measurements.

TEM measurements were made on aggregated samples of ZAD5-AuNP and ZAD7-AuNP (described in Methods section). Interparticle separations *S* were measured only from small aggregates. Representative TEM micrograph images of these small aggregates are shown in Figure 9A and 9B. The image processing was performed using *ImageJ*.[144] Each AuNP was labeled with an index *n*, and the position of the centroid $\mathbf{R}_n$ was determined. The centroid-to-centroid separation for each AuNP pair (*m*,*n*) is $|\mathbf{R}_m - \mathbf{R}_n|$. The average Feret radius (r_n) was determined individually for each particle using *ImageJ*. For a given pair of particles *m* and *n*, the interparticle separation (*S*) was determined as $S_{mn} = |\mathbf{R}_m - \mathbf{R}_n| - (r_m + r_n)$. Finally, only values of interparticle separation less than the average AuNP diameter (S_{mn} < 13.5 nm) were used to identify nearest neighbors selected for the statistical analysis of pair separation. This yielded 216 and 143 unique pairs for ZAD5-AuNP and ZAD7-AuNP, respectively. The average values are $\langle S \rangle = 2.8 \pm 0.1$ nm for ZAD5-AuNP and $\langle S \rangle = 4.3 \pm 0.2$ nm for ZAD7-AuNP (uncertainties are two times the standard deviation of the mean). It is worth noting that the average interparticle separations are highly reproducible in multiple measurements. Although the average separations are distinct, a range of separations are observed for each system: the standard deviations are 0.8 nm and 1.1 nm for ZAD5-AuNP and ZAD7-AuNP, respectively (Figure 9).

The histograms in Figure 9 show the distributions of measured separations and incorporate renderings of ZAD5 and ZAD7 on the same length scale as the histograms. Importantly, no values of *S* are observed among nearest neighbor particles that exceed the length of the model protein structures. The lengths of the model structures were measured as the distance between the C-termini of the dimeric structure, yielding 5.3 nm and 7.3 nm for ZAD5 and ZAD7, respectively. In each case, the folded protein's length coincides with the upper bound on the interparticle separation *S*. The maximum observed *S* is consistent with a single designed helical protein structure forming the linkage between adjacent AuNPs. The majority of *S* values are shorter than the length of the folded protein, presumably due to the flexibility of the GGGC linker, incomplete folding, or the formation of multiple homodimers across adjacent AuNP interfaces (Figure 10). As discussed previously, the step-like metal-binding behavior (Figure 3) is consistent with multiple

connections between AuNPs. ZAD7-AuNP has a broader distribution of pair separations, as may be expected for the longer protein and the potential for multiple linkages between particles. Distributions of pair separations with features similar to those of Figure 9 have also been observed between pairs of DNA-linked nanoparticles.[145] Lastly, the separations observed for ZAD5-AuNP and ZAD7-AuNP are consistent with the antiparallel orientation of the computational design since much smaller separations would be expected if a parallel dimer were formed. The TEM measurements necessarily involve dried samples and therefore it may not reflect the interparticle separations in solution phase.

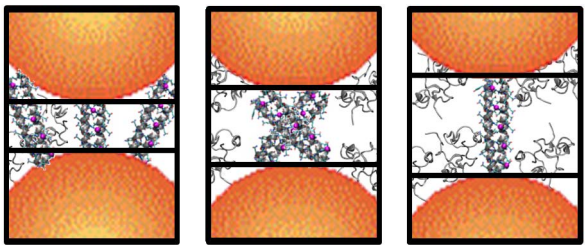

Figure 10. Effect of multiple protein linkages on particle separation. Adjacent nanoparticles can potentially be linked by one or more intervening proteins, leading to a range of pair separations.

Conclusion

A protein system was computationally designed to bind Zn^{2+} cooperatively and form an antiparallel homodimer, which could be used to functionalize gold nanoparticles (AuNPs). The targeted dimerization involves multiple metal-ion binding sites, and the periodicity of the coiled-coil structure allows control of the protein length. The sequence undergoes a transition from unstructured to alpha-helical when Zn^{2+} is introduced into the solution. The cooperative formation of helical structure is reversible with stoichiometric additions of the chelator EDTA. The designed sequence was augmented with a C-terminal cysteine linker, which allowed attachment to the AuNP surface. The resulting protein functionalized nanoparticles, ZAD5-AuNP, exhibited reversible interparticle association/dissociation. The change in AuNP separation, induced by dimerization of the ligated protein, was monitored by shifts in the surface plasmon resonance and visualized using TEM. Aqueous titrations with Zn^{2+} revealed sharp "switch-like" sigmoidal transitions over submicromolar Zn^{2+} concentrations. In addition, the metal-ion concentration that yielded nanoparticle association could be shifted by varying one of several parameters: the surface loading of the protein, solution ionic strength, addition of hydrophobic co-solvents, and the metal ion used to trigger the dimerization. The cooperativity for nanoparticle association is consistent with the multiple metal binding sites in a single dimer, folding of the dimer protein, and the association of multiple dimers between adjacent nanoparticles. The association of ZAD5-AuNP was most sensitive to Zn^{2+}, and the concentration of nanoparticle association for Zn^{2+} was well separated from those observed for La^{3+} and Mn^{2+} (Figure 4). The protein dimer length is variable with the addition or removal of repeat units within the sequence. The 5-heptad protein was lengthened by two-heptads to create a 7-heptad variant, which was used to functionalize the particles (ZAD7-AuNP). ZAD7-AuNP also exhibited reversible metal-induced nanoparticle association. For the associated states of ZAD5-AuNP and ZAD7-AuNP, TEM and extinction data were consistent with the nanoparticle separations expected given the lengths of model structures of the proteins.

While high-resolution structures of the designed proteins on the nanoparticle surfaces have not been determined, many of the experimental observations are consistent with the model structures of the designed sequences. The isolated protein ZAD5-NoLinker undergoes a transition to alpha helical structure upon exposure to Zn^{2+}. Analytical ultracentrifugation studies are consistent with monomer-dimer equilibrium at high concentrations of Zn^{2+}. The functionalized particles undergo zinc-mediated association. Solution conditions were modified with the addition of a hydrophobic co-solvent or an increase of solution ionic strength, and the subsequent increases in the Zn^{2+} concentrations necessary to elicit association were consistent with destabilization of the designed valine zipper and the salt-bridging interactions present in the computational model of the dimer. TEM measurements revealed that the distributions of interparticle separations are commensurate with the lengths of the protein model structures. Nonetheless, it will be of interest to further investigate the structure of these designed zinc binding proteins when on the AuNP and how the structure may be modified when metal ions other than Zn^{2+} are employed at high concentrations.

This *de novo* designed protein system is a step towards developing a predictive understanding of how to use large conformationally flexible amino acid sequences to create self-assembled systems with well-structured local environments. Although not explored herein, the assembly properties of the dimer proteins should also be sensitive to pH and temperature. Herein the proteins were realized using peptide synthesis, but these sequences can also be genetically encoded and fused with other proteins, thus providing a means to reversibly immobilize targeted proteins on nanoparticles. The designed proteins may also potentially be displayed on phage or cellular exteriors to provide reversible linkages to proteins and nanoparticles. Incorporating computational design of the biological component of these hybrid systems affords great control over the resultant function of the hybrid material and allows the creation of function beyond what may be leveraged with natural proteins.

AUTHOR INFORMATION

Corresponding Author

* To whom correspondence should be addressed. E-mail: saven@sas.upenn.edu (J.G.S), sojungpark@ewha.ac.kr (S.-J.P.)

Present Addresses

c. Glaxo Smith Kline, 1250 South Collegeville Road, Collegeville. PA 19426
d. Department of Chemistry and Clean Energy Institute, University of Washington, Seattle, WA 98195
e. Green Biologics Inc. 10338 Stony Run Lane, Ashland, VA 23005

Author Contributions

‡M.J.E. and C.M.M. contributed equally.

Funding Sources

The authors acknowledge support from National Science Foundation (NSF) under award CHE 1508318; the authors also acknowledge partial support from the NSF DMREF program (DMR-1234161) and from CHE-1413333. J.G.S. acknowledges additional support from the Penn Laboratory for Research on the Structure of Matter (NSF DMR-1120901), the National Institutes of Health (R01 GM-071628, R01 HL-085303). S.-J. P. acknowledges the support from the National Research Foundation of Korea grant funded by the Korea government (MSIP) (NRF-2015R1A2A2A01003528). This work used the Extreme Science and Engineering Discovery Environment (XSEDE), which is supported by National Science Foundation grant number ACI-1053575, under grant number TG-CHE110041.

ACKNOWLEDGMENT

We thank Benjamin T. Diroll for assistance with SAXS studies on the citrate capped AuNPs. We thank Daniel A. Hammer for useful discussions. We thank Ronen Marmorstein and Michael Grasso for assistance in collection of the AUC data.

SUPPORTING INFORMATION

Additional experimental methods information including protein synthesis and purification, AuNP preparation, and SAXS measurements. ZAD5 fluorescence for determining protein loading on AuNPs. Sedimentation equilibrium analytic ultracentrifugation (AUC) data. Additional details of protein structure and sequence design. CD spectra of a designed His-coordinating protein. UV-Vis λmax vs. Zn^{2+} titration for ZAD5-AuNP and ZAD7-AuNP. Control Zn^{2+} titrations into ZAD5-NoLinker citrate capped AuNP solutions. UV-Vis spectrum of Zn^{2+} saturated ZAD5-AuNP and ZAD7-AuNP. This information is available free of charge via the internet at http://pubs.acs.org

REFERENCES

(1) Pinaud, F.; King, D.; Moore, H. P.; Weiss, S., *J. Am. Chem. Soc.* **2004,** *126* (19), 6115-6123.
(2) Bastus, N. G.; Sanchez-Tillo, E.; Pujals, S.; Farrera, C.; Lopez, C.; Giralt, E.; Celada, A.; Lloberas, J.; Puntes, V., *Acs Nano* **2009,** *3* (6), 1335-1344.
(3) Liu, M.; Fu, J.; Hejesen, C.; Yang, Y.; Woodbury, N. W.; Gothelf, K.; Liu, Y.; Yan, H., *Nat. Commun.* **2013,** *4* (DOI: 10.1038/ncomms3127).
(4) Zhang, X.; Wang, R.; Xue, G., *Soft Matter* **2015,** *11* (10), 1862-1870.
(5) Yang, L.; Zhang, X.; Ye, M.; Jiang, J.; Yang, R.; Fu, T.; Chen, Y.; Wang, K.; Liu, C.; Tan, W., *Adv. Drug Del. Rev.* **2011,** *63* (14-15), 1361-1370.
(6) Buckhout-White, S.; Spillmann, C. M.; Algar, W. R.; Khachatrian, A.; Melinger, J. S.; Goldman, E. R.; Ancona, M. G.; Medintz, I. L., *Nat. Commun.* **2014,** *5* (DOI: 10.1038/ncomms6615).
(7) Murray, C. B.; Kagan, C. R.; Bawendi, M. G., *Annu. Rev. Mater. Sci.* **2000,** *30*, 545-610.
(8) Kamat, P. V., *J. Phys. Chem. B* **2002,** *106* (32), 7729-7744.
(9) Katz, E.; Willner, I., *Angew. Chem. Int. Ed.* **2004,** *43* (45), 6042-6108.
(10) Lu, A. H.; Salabas, E. L.; Schuth, F., *Angew. Chem. Int. Ed.* **2007,** *46* (8), 1222-1244.
(11) Li, N.; Zhao, P. X.; Astruc, D., *Angew. Chem. Int. Ed.* **2014,** *53* (7), 1756-1789.
(12) Qian, Z. X.; Hastings, S. P.; Li, C.; Edward, B.; McGinn, C. K.; Engheta, N.; Fakhraai, Z.; Park, S. J., *Acs Nano* **2015,** *9* (2), 1263-1270.
(13) Hayat, M. A., Wiley Periodicals, Inc.: 1991.
(14) Zhao, P.; Li, N.; Astruc, D., *Coord. Chem. Rev.* **2013,** *257* (3-4), 638-665.
(15) Sandstrom, P.; Boncheva, M.; Akerman, B., *Langmuir* **2003,** *19* (18), 7537-7543.
(16) Pellegrino, T.; Sperling, R. A.; Alivisatos, A. P.; Parak, W. J., *J. Biomed. Biotechnol.* **2007,** (DOI: 10.1155/2007/26796).
(17) Cedervall, T.; Lynch, I.; Lindman, S.; Berggard, T.; Thulin, E.; Nilsson, H.; Dawson, K. A.; Linse, S., *Proc. Natl. Acad. Sci. USA* **2007,** *104* (7), 2050-2055.
(18) Lane, L. A.; Qian, X.; Smith, A. M.; Nie, S., *Annual Review of Physical Chemistry, Vol 66* **2015,** *66*, 521-547.
(19) Zhao, W.; Brook, M. A.; Li, Y., *Chembiochem* **2008,** *9* (15), 2363-2371.
(20) Taylor, R. W.; Lee, T.-C.; Scherman, O. A.; Esteban, R.; Aizpurua, J.; Huang, F. M.; Baumberg, J. J.; Mahajan, S., *Acs Nano* **2011,** *5* (5), 3878-3887.
(21) Xia, H.; Su, G.; Wang, D., *Angew. Chem. Int. Ed.* **2013,** *52* (13), 3726-3730.
(22) Yang, M.; Chen, G.; Zhao, Y.; Silber, G.; Wang, Y.; Xing, S.; Han, Y.; Chen, H., *PCCP* **2010,** *12* (38), 11850-11860.
(23) Alivisatos, A. P.; Johnsson, K. P.; Peng, X. G.; Wilson, T. E.; Loweth, C. J.; Bruchez, M. P.; Schultz, P. G., *Nature* **1996,** *382* (6592), 609-611.
(24) Mirkin, C. A.; Letsinger, R. L.; Mucic, R. C.; Storhoff, J. J., *Nature* **1996,** *382* (6592), 607-609.
(25) Sastry, M.; Kumar, A.; Datar, S.; Dharmadhikari, C. V.; Ganesh, K. N., *Appl. Phys. Lett.* **2001,** *78* (19), 2943-2945.
(26) Maeda, Y.; Tabata, H.; Kawai, T., *Appl. Phys. Lett.* **2001,** *79* (8), 1181-1183.
(27) Taton, T. A.; Mucic, R. C.; Mirkin, C. A.; Letsinger, R. L., *J. Am. Chem. Soc.* **2000,** *122* (26), 6305-6306.
(28) Senesi, A. J.; Eichelsdoerfer, D. J.; Macfarlane, R. J.; Jones, M. R.; Auyeung, E.; Lee, B.; Mirkin, C. A., *Angew. Chem. Int. Ed.* **2013,** *52* (26), 6624-6628.
(29) Auyeung, E.; Li, T. I. N. G.; Senesi, A. J.; Schmucker, A. L.; Pals, B. C.; de la Cruz, M. O.; Mirkin, C. A., *Nature* **2014,** *505* (7481), 73-77.
(30) Dujardin, E.; Hsin, L. B.; Wang, C. R. C.; Mann, S., *Chem. Commun.* **2001,** (14), 1264-1265.
(31) Yao, H.; Yi, C.; Tzang, C.-H.; Zhu, J.; Yang, M., *Nanotechnology* **2007,** *18* (1).

(32) Schreiber, R.; Do, J.; Roller, E.-M.; Zhang, T.; Schueller, V. J.; Nickels, P. C.; Feldmann, J.; Liedl, T., *Nat. Nanotechnol.* **2014,** *9* (1), 74-78.
(33) Loweth, C. J.; Caldwell, W. B.; Peng, X. G.; Alivisatos, A. P.; Schultz, P. G., *Angew. Chem. Int. Ed.* **1999,** *38* (12), 1808-1812.
(34) Shim, T. S.; Estephan, Z. G.; Qian, Z. X.; Prosser, J. H.; Lee, S. Y.; Chenoweth, D. M.; Lee, D.; Park, S. J.; Crocker, J. C., *Nat. Nanotechnol.* **2017,** *12* (1), 41-47.
(35) Estephan, Z. G.; Qian, Z. X.; Lee, D.; Crocker, J. C.; Park, S. J., *Nano Lett.* **2013,** *13* (9), 4449-4455.
(36) Yu, X.; Lei, D. Y.; Amin, F.; Hartmann, R.; Acuna, G. P.; Guerrero-Martinez, A.; Maier, S. A.; Tinnefeld, P.; Carregal-Romero, S.; Parak, W. J., *Nano Today* **2013,** *8* (5), 480-493.
(37) Clausen-Schaumann, H.; Rief, M.; Tolksdorf, C.; Gaub, H. E., *Biophys. J.* **2000,** *78* (4), 1997-2007.
(38) Yakovchuk, P.; Protozanova, E.; Frank-Kamenetskii, M. D., *Nucleic Acids Res.* **2006,** *34* (2), 564-574.
(39) Wei, X. X.; Nangreave, J.; Liu, Y., *Acc. Chem. Res.* **2014,** *47* (6), 1861-1870.
(40) Kulakovich, O.; Strekal, N.; Yaroshevich, A.; Maskevich, S.; Gaponenko, S.; Nabiev, I.; Woggon, U.; Artemyev, M., *Nano Lett.* **2002,** *2* (12), 1449-1452.
(41) Zhao, W.-W.; Yu, P.-P.; Shan, Y.; Wang, J.; Xu, J.-J.; Chen, H.-Y., *Anal. Chem.* **2012,** *84* (14), 5892-5897.
(42) Shimron, S.; Cecconello, A.; Lu, C.-H.; Willner, I., *Nano Lett.* **2013,** *13* (8), 3791-3795.
(43) Wang, J.; Shan, Y.; Zhao, W.-W.; Xu, J.-J.; Chen, H.-Y., *Anal. Chem.* **2011,** *83* (11), 4004-4011.
(44) Ma, Z.-Y.; Ruan, Y.-F.; Xu, F.; Zhao, W.-W.; Xu, J.-J.; Chen, H.-Y., *Anal. Chem.* **2016,** *88* (7), 3864-3871.
(45) Ahn, J.; Choi, Y.; Lee, A.-R.; Lee, J.-H.; Jung, J. H., *Analyst* **2016,** *141* (6), 2040-2045.
(46) Sun, W.; Lu, Y.; Mao, J.; Chang, N.; Yang, J.; Liu, Y., *Anal. Chem.* **2015,** *87* (6), 3354-3359.
(47) Wang, W.; Chen, C.; Qian, M.; Zhao, X. S., *Anal. Biochem.* **2008,** *373* (2), 213-219.
(48) Li, F.; Zhang, H.; Lai, C.; Li, X.-F.; Le, X. C., *Angew. Chem. Int. Ed.* **2012,** *51* (37), 9317-9320.
(49) Park, D. H.; Lee, J.-S., *Electron. Mater. Lett.* **2015,** *11* (3), 336-345.
(50) Connolly, S.; Fitzmaurice, D., *Adv. Mater.* **1999,** *11* (14), 1202-1205.
(51) Aili, D.; Gryko, P.; Sepulveda, B.; Dick, J. A. G.; Kirby, N.; Heenan, R.; Baltzer, L.; Liedberg, B.; Ryan, M. P.; Stevens, M. M., *Nano Lett.* **2011,** *11* (12), 5564-5573.
(52) Fu, X. Y.; Wang, Y.; Huang, L. X.; Sha, Y. L.; Gui, L. L.; Lai, L. H.; Tang, Y. Q., *Adv. Mater.* **2003,** *15* (11), 902-+.
(53) Tuan Anh, P.; Schreiber, A.; Sturm, E. V.; Schiller, S.; Coelfen, H., *Beilstein J. Nanotechnol.* **2016,** *7*, 351-363.
(54) Chang, J.-B.; Kim, Y. H.; Thompson, E.; No, Y. H.; Kim, N. H.; Arrieta, J.; Manfrinato, V. R.; Keating, A. E.; Berggren, K. K., *Small* **2016,** *12* (11), 1498-1505.
(55) Dominguez-Medina, S.; Kisley, L.; Tauzin, L. J.; Hoggard, A.; Shuang, B.; Indrasekara, A.; Chen, S. S.; Wang, L. Y.; Derry, P. J.; Liopo, A.; Zubarev, E. R.; Landes, C. F.; Link, S., *Acs Nano* **2016,** *10* (2), 2103-2112.
(56) Dominguez-Medina, S.; Blankenburg, J.; Olson, J.; Landes, C. F.; Link, S., *ACS Sustainable Chem. Eng.* **2013,** *1* (7), 833-842.
(57) Chanana, M.; Correa-Duarte, M. A.; Liz-Marzan, L. M., *Small* **2011,** *7* (18), 2650-2660.
(58) Rio-Echevarria, I. M.; Tavano, R.; Causin, V.; Papini, E.; Mancin, F.; Moretto, A., *J. Am. Chem. Soc.* **2011,** *133* (1), 8-11.
(59) Chen, P.; Selegard, R.; Aili, D.; Liedberg, B., *Nanoscale* **2013,** *5* (19), 8973-8976.
(60) Liu, F.; Xue, L.; Yuan, Y.; Pan, J.; Zhang, C.; Wang, H.; Brash, J. L.; Yuan, L.; Chen, H., *Nanoscale* **2016,** *8* (7), 4387-4394.
(61) Yamamoto, S.; Nakanishi, J.; Yamaguchi, K., *J. Photopolym. Sci. Technol.* **2015,** *28* (2), 269-272.
(62) Kaur, P.; Maeda, Y.; Mutter, A. C.; Matsunaga, T.; Xu, Y.; Matsui, H., In *Angew. Chem. Int. Ed.*, WILEY-VCH Verlag: 2010; Vol. 49, pp 8375-8378.
(63) Sharma, N.; Top, A.; Kiick, K. L.; Pochan, D. J., In *Angew. Chem. Int. Ed.*, WILEY-VCH Verlag: 2009; Vol. 48, pp 7078-7082.
(64) McMillan, R. A.; Paavola, C. D.; Howard, J.; Chan, S. L.; Zaluzec, N. J.; Trent, J. D., In *Nature Materials*, Nature Publishing Group: 2002; Vol. 1, pp 247-252.
(65) Srivastava, S.; Samanta, B.; Jordan, B. J.; Hong, R.; Xiao, Q.; Tuominen, M. T.; Rotello, V. M., In *J. Am. Chem. Soc.*, American Chemical Society: 2007; Vol. 129, pp 11776-11780.
(66) Tang, J.; Badelt-Lichtblau, H.; Ebner, A.; Preiner, J.; Kraxberger, B.; Gruber, H. J.; Sleytr, U. B.; Ilk, N.; Hinterdorfer, P., In *ChemPhysChem*, WILEY-VCH Verlag: 2008; Vol. 9, pp 2317-2320.
(67) Hwang, L.; Chen, C.-L.; Rosi, N. L., In *Chem. Commun.*, The Royal Society of Chemistry: 2011; Vol. 47, pp 185-187.
(68) Chah, S.; Hammond, M. R.; Zare, R. N., In *Chem. Biol.*, 2005; Vol. 12, pp 323-328.
(69) Bayraktar, H.; Srivastava, S.; You, C.-C.; Rotello, V. M.; Knapp, M. J., In *Soft Matter*, Royal Society of Chemistry: 2008; Vol. 4, pp 751-756.
(70) Wagner, S. C.; Roskamp, M.; Cölfen, H.; Böttcher, C.; Schlecht, S.; Koksch, B., In *Org. Biomol. Chem.*, 2009; Vol. 7, pp 46-51.
(71) Schöne, D.; Schade, B.; Böttcher, C.; Koksch, B., In *Beilstein J Org Chem*, Beilstein-Institut: 2015; Vol. 11, pp 792-803.
(72) You, C.-C.; De, M.; Rotello, V. M., In *Curr. Opin. Chem. Biol.*, 2005; Vol. 9, pp 639-646.
(73) Zhou, G.; Liu, Y.; Luo, M.; Li, X.; Xu, Q.; Ji, X.; He, Z., In *Langmuir*, American Chemical Society: 2013; Vol. 29, pp 4697-4702.
(74) Katz, E.; Willner, I., In *Angew. Chem. Int. Ed.*, WILEY-VCH Verlag: 2004; Vol. 43, pp 6042-6108.
(75) Si, S.; Mandal, T. K., In *Langmuir*, 2007; Vol. 23, pp 190-195.
(76) Graf, P.; Mantion, A.; Foelske, A.; Shkilnyy, A.; Mašić, A.; Thünemann, A. F.; Taubert, A., *Chem. Eur. J.* **2009,** *15* (23), 5831-5844.
(77) Manikas, A. C.; Causa, F.; Della Moglie, R.; Netti, P. A., *ACS Appl. Mater. Interfaces* **2013,** *5* (16), 7915-7922.
(78) Stevens, M. M.; Flynn, N. T.; Wang, C.; Tirrell, D. A.; Langer, R., In *Adv. Mater. Weinheim*, WILEY-VCH Verlag: 2004; Vol. 16, pp 915-918.
(79) Ryadnov, M. G.; Ceyhan, B.; Niemeyer, C. M.; Woolfson, D. N., *J. Am. Chem. Soc.* **2003,** *125* (31), 9388-9394.
(80) Aili, D.; Selegård, R.; Baltzer, L.; Enander, K.; Liedberg, B., In *Small*, WILEY-VCH Verlag: 2009; Vol. 5, pp 2445-2452.
(81) Aili, D.; Gryko, P.; Sepulveda, B.; Dick, J. A. G.; Kirby, N.; Heenan, R.; Baltzer, L.; Liedberg, B.; Ryan, M. P.; Stevens, M. M., *Nano Lett.* **2011,** *11* (12), 5564-5573.
(82) Aili, D.; Enander, K.; Rydberg, J.; Nesterenko, I.; Björefors, F.; Baltzer, L.; Liedberg, B., In *J. Am. Chem. Soc.*, 2008; Vol. 130, pp 5780-5788.
(83) Floudas, C. A.; Fung, H. K.; McAllister, S. R.; Monnigmann, M.; Rajgaria, R., *Chem. Eng. Sci.* **2006,** *61* (3), 966-988.

(84) Dill, K. A.; Ozkan, S. B.; Shell, M. S.; Weikl, T. R., In *Annu. Rev. Biophys.*, Annual Reviews: Palo Alto, 2008; Vol. 37, pp 289-316.

(85) Lu, Y.; Yeung, N.; Sieracki, N.; Marshall, N. M., *Nature* **2009,** *460* (7257), 855-862.

(86) Samish, I.; MacDermaid, C. M.; Perez-Aguilar, J. M.; Saven, J. G., In *Annual Review of Physical Chemistry, Vol 62*, Leone, S. R.; Cremer, P. S.; Groves, J. T.; Johnson, M. A., Eds. Annual Reviews: Palo Alto, 2011; Vol. 62, pp 129-149.

(87) Woolfson, D. N., *Fibrous Proteins: Coiled-Coils, Collagen and Elastomers* **2005,** *70*, 79-112.

(88) North, B.; Summa, C. M.; Ghirlanda, G.; DeGrado, W. F., *J. Mol. Biol.* **2001,** *311* (5), 1081-1090.

(89) Grigoryan, G.; DeGrado, W. F., *J. Mol. Biol.* **2011,** *405* (4), 1079-1100.

(90) Huang, P. S.; Oberdorfer, G.; Xu, C. F.; Pei, X. Y.; Nannenga, B. L.; Rogers, J. M.; DiMaio, F.; Gonen, T.; Luisi, B.; Baker, D., *Science* **2014,** *346* (6208), 481-485.

(91) Thomson, A. R.; Wood, C. W.; Burton, A. J.; Bartlett, G. J.; Sessions, R. B.; Brady, R. L.; Woolfson, D. N., *Science* **2014,** *346* (6208), 485-488.

(92) Araghi, R. R.; Keating, A. E., *Curr. Opin. Struct. Biol.* **2016,** *39*, 27-38.

(93) Dublin, S. N.; Conticello, V. P., *J. Am. Chem. Soc.* **2008,** *130* (1), 49-51.

(94) Der, B. S.; Jha, R. K.; Lewis, S. M.; Thompson, P. M.; Guntas, G.; Kuhlman, B., *Proteins* **2013,** *81* (7), 1245-55.

(95) Mocny, C. S.; Pecoraro, V. L., *Acc. Chem. Res.* **2015,** *48* (8), 2388-96.

(96) Chino, M.; Maglio, O.; Nastri, F.; Pavone, V.; DeGrado, W. F.; Lombardi, A., *Eur. J. Inorg. Chem.* **2015,** *2015* (21), 3371-3390.

(97) Brodin, J. D.; Ambroggio, X. I.; Tang, C. Y.; Parent, K. N.; Baker, T. S.; Tezcan, F. A., *Nature Chemistry* **2012,** *4* (5), 375-382.

(98) Turkevich, J.; Stevenson, P. C.; Hillier, J., *J. Phys. Chem.* **1953,** *57* (7), 670-673.

(99) Zhang, X.; Servos, M. R.; Liu, J. W., *J. Am. Chem. Soc.* **2012,** *134* (24), 9910-9913.

(100) Enustun, B. V.; Turkevich, J., *J. Am. Chem. Soc.* **1963,** *85* (21), 12.

(101) Turkevich, J., *Gold Bulletin* **1985,** *18* (3), 86-91.

(102) Polavarapu, L.; Xu, Q. H., *Nanotechnology* **2009,** *20* (18), 7.

(103) Grabar, K. C.; Freeman, R. G.; Hommer, M. B.; Natan, M. J., *Anal. Chem.* **1995,** *67* (4), 735-743.

(104) Storhoff, J. J.; Elghanian, R.; Mucic, R. C.; Mirkin, C. A.; Letsinger, R. L., *J. Am. Chem. Soc.* **1998,** *120* (9), 1959-1964.

(105) Zhang, F. X.; Han, L.; Israel, L. B.; Daras, J. G.; Maye, M. M.; Ly, N. K.; Zhong, C. J., *Analyst* **2002,** *127* (4), 462-465.

(106) Li, Z.; Jin, R. C.; Mirkin, C. A.; Letsinger, R. L., *Nucleic Acids Res.* **2002,** *30* (7), 1558-1562.

(107) Letsinger, R. L.; Elghanian, R.; Viswanadham, G.; Mirkin, C. A., *Bioconjugate Chem.* **2000,** *11* (2), 289-291.

(108) Demers, L. M.; Mirkin, C. A.; Mucic, R. C.; Reynolds, R. A.; Letsinger, R. L.; Elghanian, R.; Viswanadham, G., *Anal. Chem.* **2000,** *72* (22), 5535-5541.

(109) Sanyal, G.; Kim, E.; Thompson, F. M.; Brady, E. K., *Biochem. Biophys. Res. Commun.* **1989,** *165* (2), 772-781.

(110) Laue, T. M.; Shah, B. D.; Ridgeway, T. M.; Pelletier, S. L., In *Analytical Ultracentrifugation in Biochemistry and Polymer Science*, Harding, S. E.; Rowe, A. J.; Horton, J. C., Eds. Royal Society of Chemistry: Cambridge, UK: 1992; p 90.

(111) Vistica, J.; Dam, J.; Balbo, A.; Yikilmaz, E.; Mariuzza, R. A.; Rouault, T. A.; Schuck, P., *Anal. Biochem.* **2004,** *326* (2), 234-256.

(112) Bryson, J. W.; Betz, S. F.; Lu, H. S.; Suich, D. J.; Zhou, H. X.; O'Neil, K. T.; DeGrado, W. F., *Science* **1995,** *270* (5238), 935-41.

(113) Harbury, P. B.; Zhang, T.; Kim, P. S.; Alber, T., *Science* **1993,** *262* (5138), 1401-1407.

(114) Crick, F. H. C., *Acta Crystallogr.* **1953,** *6* (8-9), 689-697.

(115) Crick, F. H. C., *Acta Crystallogr.* **1953,** *6* (8-9), 685-689.

(116) Humphrey, W.; Dalke, A.; Schulten, K., *J. Mol. Graphics Modell.* **1996,** *14* (1), 33-38.

(117) MacDermaid, C. M. Coiled-Coil Builder Plugin for Visual Molecular Dynamics (VMD). https://github.com/CoiledCoilBuilder.

(118) Krantz, B. A.; Sosnick, T. R., *Nat. Struct. Biol.* **2001,** *8* (12), 1042-1047.

(119) Ghadiri, M. R.; Choi, C., *J. Am. Chem. Soc.* **1990,** *112* (4), 1630-1632.

(120) Kono, H.; Saven, J. G., *J. Mol. Biol.* **2001,** *306* (3), 607-628.

(121) Calhoun, J. R.; Kono, H.; Lahr, S.; Wang, W.; DeGrado, W. F.; Saven, J. G., *J. Mol. Biol.* **2003,** *334* (5), 1101-1115.

(122) Bender, G. M.; Lehmann, A.; Zou, H.; Cheng, H.; Fry, H. C.; Engel, D.; Therien, M. J.; Blasie, J. K.; Roder, H.; Saven, J. G.; DeGrado, W. F., *J. Am. Chem. Soc.* **2007,** *129* (35), 10732-10740.

(123) Lanci, C. J.; MacDermaid, C. M.; Kang, S. G.; Acharya, R.; North, B.; Yang, X.; Qiu, X. J.; DeGrado, W. F.; Saven, J. G., *Proc. Natl. Acad. Sci. USA* **2012,** *109* (19), 7304-7309.

(124) Dunbrack, R. L., *Curr. Opin. Struct. Biol.* **2002,** *12* (4), 431-440.

(125) Fry, H. C.; Lehmann, A.; Saven, J. G.; DeGrado, W. F.; Therien, M. J., *J. Am. Chem. Soc.* **2010,** *132* (11), 3997-4005.

(126) Fry, H. C.; Lehmann, A.; Sinks, L. E.; Asselberghs, I.; Tronin, A.; Krishnan, V.; Blasie, J. K.; Clays, K.; DeGrado, W. F.; Saven, J. G.; Therien, M. J., *J. Am. Chem. Soc.* **2013,** *135* (37), 13914-13926.

(127) Minelli, C.; Liew, J. X.; Muthu, M.; Andresen, H., *Soft Matter* **2013,** *9* (20), 5119-5124.

(128) Mulvaney, P., *Langmuir* **1996,** *12* (3), 788-800.

(129) Yonzon, C. R.; Jeoungf, E.; Zou, S. L.; Schatz, G. C.; Mrksich, M.; Van Duyne, R. P., *J. Am. Chem. Soc.* **2004,** *126* (39), 12669-12676.

(130) Kelly, K. L.; Coronado, E.; Zhao, L. L.; Schatz, G. C., *J. Phys. Chem. B* **2003,** *107* (3), 668-677.

(131) Shipway, A. N.; Lahav, M.; Gabai, R.; Willner, I., *Langmuir* **2000,** *16* (23), 8789-8795.

(132) Verma, A.; Srivastava, S.; Rotello, V. M., *Chem. Mater.* **2005,** *17* (25), 6317-6322.

(133) Sonnichsen, C.; Reinhard, B. M.; Liphardt, J.; Alivisatos, A. P., *Nat. Biotechnol.* **2005,** *23* (6), 741-745.

(134) Thanh, N. T. K.; Rosenzweig, Z., *Anal. Chem.* **2002,** *74* (7), 1624-1628.

(135) Lu, C. H.; Lin, Y. F.; Lin, J. J.; Yu, C. S., *Plos One* **2012,** *7* (6), 12.

(136) Irving, H.; Williams, R. J. P., *Nature* **1948,** *162* (4123), 746-747.

(137) Irving, H.; Williams, R. J. P., *J. Chem. Soc.* **1953,** (OCT), 3192-3210.

(138) Dudev, M.; Wang, J.; Dudev, T.; Lim, C., *J. Phys. Chem. B* **2006,** *110* (4), 1889-1895.

(139) Hancock, R. D.; Martell, A. E., *Chem. Rev.* **1989,** *89* (8), 1875-1914.

(140) Peacock, A. F. A., In *Peptide, Protein and Enzyme Design*, Pecoraro, V. L., Ed. Elsevier Academic Press Inc: San Diego, 2016; Vol. 580, pp 557-580.

(141) Sonnichsen, F. D.; Vaneyk, J. E.; Hodges, R. S.; Sykes, B. D., *Biochemistry* **1992,** *31* (37), 8790-8798.
(142) Buck, M., *Q. Rev. Biophys.* **1998,** *31* (3), 297-355.
(143) Luo, P. Z.; Baldwin, R. L., *Biochemistry* **1997,** *36* (27), 8413-8421.
(144) Schneider, C. A.; Rasband, W. S.; Eliceiri, K. W., *Nat. Methods* **2012,** *9* (7), 671-675.
(145) Zanchet, D.; Micheel, C. M.; Parak, W. J.; Gerion, D.; Williams, S. C.; Alivisatos, A. P., *J. Phys. Chem. B* **2002,** *106* (45), 11758-11763.